

On the optical emission in the mini-outburst of the black hole X-ray binary MAXI J1348-630

XIAO FAN,¹ BEI YOU,¹ DIZHAN DU,² HAN HE,¹ AND SHUAIKANG YANG¹

¹*Department of Astronomy, School of Physics and Technology, Wuhan University, Wuhan 430072, People's Republic of China*

²*Institute for Astronomy, School of Physics, Zhejiang University, Hangzhou 310058, China*

ABSTRACT

We present a multi-wavelength study on the mini-outburst of the black hole X-ray binary MAXI J1348-630 to investigate the origin of its optical emission. Using the X-ray data from Insight-HXMT and the optical observations from the Las Cumbres Observatory, we find a power-law correlation between the optical and X-ray fluxes with slopes of ~ 0.4 , indicating a hybrid contribution to the optical emission from both viscously heated disk and irradiation of the outer disk illuminated by the inner X-ray emission, but inconsistent with jet-dominated optical emission. Time delay analysis shows that the optical emission precedes the X-ray by ~ 8.5 days, which can be naturally interpreted by the disk instability model (DIM). Meanwhile, spectral energy distribution (SED) fitting with an irradiated disk model successfully reproduces the observed optical and X-ray emission, with negligible contribution from the jet. The color-magnitude diagram further supports the disk-dominated optical origin of MAXI J1348-630 during its mini-outburst. Our results suggest that the DIM plays a central role in understanding mini-outbursts of X-ray binaries.

Keywords: Stellar mass black holes; Accretion; X-ray binaries; Optical Emission

1. INTRODUCTION

During an outburst of low-mass X-ray binaries (LMXBs), a compact object (e.g., black hole in this work) accretes material through Roche lobe overflow from a companion star with mass $\lesssim 1 M_{\odot}$, emitting large amounts of radiation from radio to the X-ray band (see Belloni & Motta 2016, for review). LMXBs are characterized by their strong X-ray emission, consisting of a thermal component originating from the inner region of the accretion disk (Shakura & Sunyaev 1973; Mitsuda et al. 1984) and a nonthermal component generally arising from a hot accretion flow or a Comptonizing corona (Zdziarski & Gierliński 2004; Sunyaev & Titarchuk 1980). Radio emissions from LMXBs are commonly attributed to synchrotron radiation originating from powerful collimated jets (Hjellming & Johnston 1988; Fender 2006). However, the origin of optical emission in LMXBs is still not fully understood, as multiple mechanisms can contribute to, including the viscous heating of the accretion disk (Yang et al. 2022; You et al.

2023), the irradiation of the outer disk by X-rays (i.e., X-ray reprocessing; van Paradijs & McClintock 1994; Rykoff et al. 2007; Gierliński et al. 2008, 2009), and the optically thin synchrotron radiation from jets (Fender 2001; Markoff et al. 2001; Homan et al. 2005; Russell et al. 2006).

DIM has been widely adopted to explain the outbursts observed in LMXBs (Lasota 2001; Dubus et al. 2001; Hameury 2020). In this framework, thermal-viscous instabilities are triggered at some place when the temperature reaches the hydrogen ionization temperature, causing a rapid increase in the temperature and mass accretion rate, which results in an outburst. Consequently, the temperature and surface density of the ionized and neutral regions undergo sharp variations in a small region known as the cooling (ionized to neutral) or heating (neutral to ionized) front. The propagation of heating and cooling fronts governs the evolution of an outburst, in which the inward-moving heating front initiates the outburst and the subsequent cooling front drives its decay (e.g., Dubus et al. 2001).

LMXBs often exhibit state transitions in X-rays, shifting between different accretion states (see Remillard & McClintock 2006, for review). These transitions are typically classified into the “low-hard state (LHS)”, where

the emission is dominated by nonthermal radiation from the Comptonization corona, and the “high-soft state (HSS)”, where the thermal emission becomes prominent (Homan & Belloni 2005). During an outburst, LMXBs typically transition from the LHS through an intermediate state to the HSS, and eventually return to the LHS, tracing a “q-shaped” trajectory in the hardness–intensity diagram (e.g., Homan et al. 2001). However, this canonical pattern is not universal: approximately 30% – 40% of outbursts either remain in the LHS throughout the entire period or enter the intermediate state but fail to transition to the HSS (so called the “failed outbursts”, Alabarta et al. 2021; Lucchini et al. 2023). The truncated disk model serves as the paradigm for understanding state transitions (Done et al. 2007; Yuan & Narayan 2014), and therefore understanding what governs the state transitions remains a central question in black hole accretion physics, which reflect fundamental changes in the geometries and dynamics of the accretion flow (e.g., Dai et al. 2023; You et al. 2021; You et al. 2023).

It is not uncommon for LMXBs to exhibit one or more secondary maxima in their light curves after the main outburst, typically with fluxes 1-2 orders of magnitude lower than the main outburst. These phenomena are often referred to as mini-outbursts (also known as reflares and re-brightenings Zhang et al. 2019; Özbey Arabacı et al. 2022; Saikia et al. 2023). The majority of mini-outbursts are analogous to a “failed outburst,” while a subset could experience state transitions (e.g., Yan & Yu 2017; Cúneo et al. 2020). Although the exact triggering mechanism of mini-outbursts and their state transitions still remain unclear, their quasi-periodic oscillation properties, state transition behavior, and light curve profiles closely resemble those of main outbursts, suggesting that they may share the same physical processes (e.g., Yan & Yu 2017; Cúneo et al. 2020; Alabarta et al. 2022; Bright et al. 2025).

MAXI J1348–630 is a recently discovered LMXB that has been high-cadence monitored across radio, optical, and X-ray bands (Yatabe et al. 2019; Russell et al. 2019a,b; Sanna et al. 2019; Chen et al. 2019). MAXI J1348–630 underwent a main outburst beginning on January 27, 2019, during which it experienced a complete state transition and then returned to quiescence on May 15, 2019. Approximately 10 days later, it experienced a mini-outburst that remained in the hard state throughout, with a peak X-ray flux approximately one order of magnitude lower than the main outburst (Negoro et al. 2019; Jana et al. 2020; Tominaga et al. 2020; Zhang et al. 2020a; Carotenuto et al. 2021). Weng et al. (2021) and You et al. (2024) have conducted comprehen-

sive multi-wavelength studies of MAXI J1348–630 during its main outburst, exploring the radiative origins across different wavebands and the evolution of accretion flow. In this work, we present a multi-wavelength study on the mini-outburst of MAXI J1348–630 and aim to investigate the origin of its optical emission, which may help us further understand the state transition process in LMXBs. In Section 3, we analyze the time delays between the optical and X-ray emissions of MAXI J1348–630, examine their flux correlation, and present the results of SED fitting. We discuss the implications for understanding the optical origin and state transitions in Section 4.

2. DATA REDUCTION

2.1. *Insight-HXMT*

Insight-HXMT is China’s first X-ray astronomical satellite launched on 2017 June 15, carrying three main payloads with different effective areas (Zhang et al. 2020b): the Low Energy telescope (LE, 384cm² at 1-12 keV), the Medium Energy telescope (ME, 952cm² at 8-35 keV), and the High Energy telescope (HE, 5100cm² at 20-350 keV). Insight-HXMT detected the mini-outburst of MAXI J1348–630 since MJD 58637 and has been continuously monitoring until MJD 58693. All X-ray data during the mini-outburst were reduced by Insight-HXMT Data Analysis Software (HXMTDAS). Following You et al. (2024), the energy bands adopted in this work are 2-10 keV (LE), 10-28 keV (ME), and 28-150 keV (HE); data in 21–24 keV were ignored due to the photoelectric effect of electrons in the silver K shell. The light curves for LE, ME, and HE are shown in Figure 1.

During the mini-outburst of MAXI J1348–630, the Comptonization flux dominates the observed X-ray emission (Zhang et al. 2020a). Therefore, we performed the spectral fitting in the X-ray using the model `tbabs*(diskbb+nthcomp)` in XSPEC and then derived the X-ray Comptonization flux through `cflux` module. The neutral hydrogen column density toward MAXI J1348–630 is taken to be $N_H = 8.6 \times 10^{21} \text{ cm}^{-2}$ (Tominaga et al. 2020). For X-ray spectral fitting of MAXI J1348–630 during its main outburst, we refer readers to You et al. (2024). The light curve of X-ray Comptonization flux is presented at the bottom of Figure 1 and the data are tabulated in Table 1.

2.2. *Las Cumbres Observatory*

The optical data were obtained from the Las Cumbres Observatory (LCO) Global Telescope, a worldwide network of telescopes designed for optical time-domain astronomy (Brown et al. 2013). LCO monitored the mini-outburst of MAXI J1348–630 starting from MJD 58624.

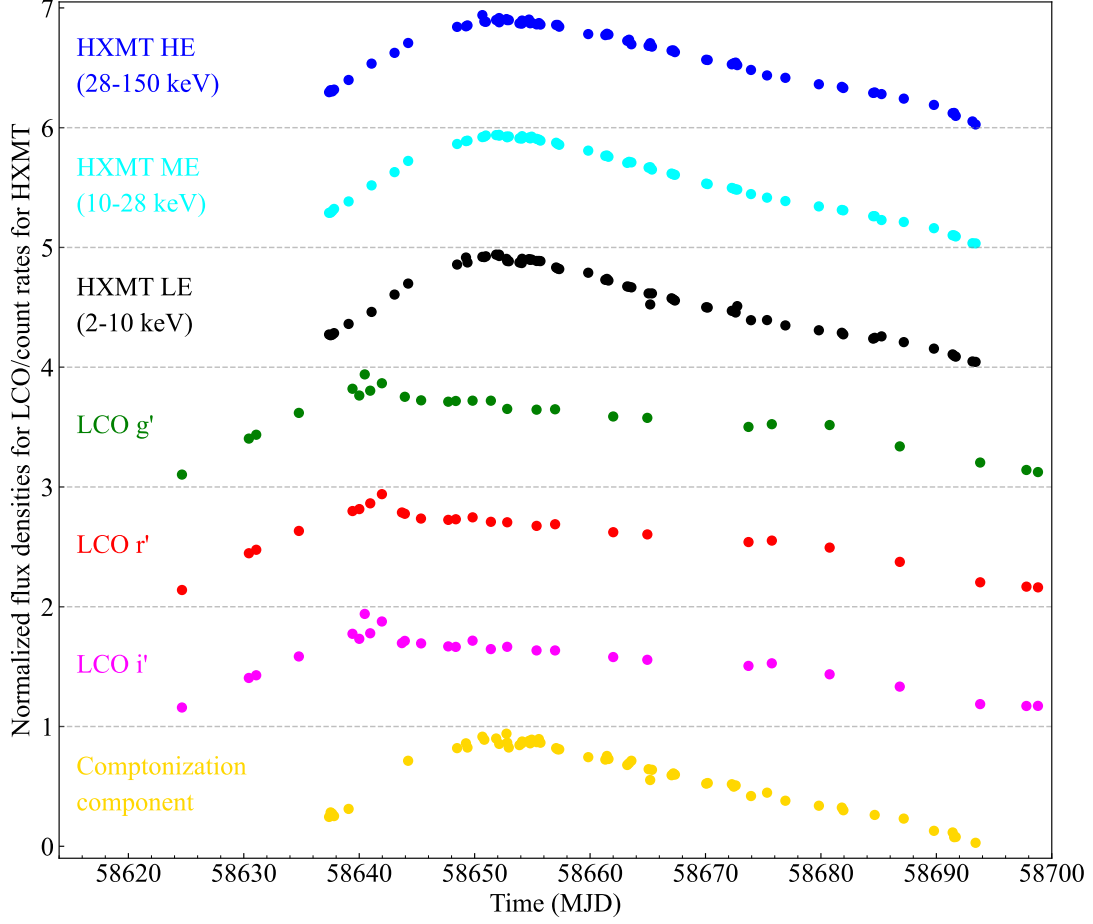


Figure 1. The light curves of MAXI J1348-630 during the mini-outburst. The count rates for Insight-HXMT and flux densities for LCO have been normalized for comparison. The bottom panel displays the Comptonization flux.

Observations were carried out using the g' , r' , and i' filters of the Sloan Digital Sky Survey (SDSS). The raw data were processed through the **BANZAI** pipeline, which provides standard image reduction. Photometric measurements were performed using the Automated Photometry of Transients pipeline (AutoPhOT; Brennan & Fraser 2022), which calculates the AB magnitudes calibrated against the SkyMapper catalog and estimates the magnitude errors based on both the signal-to-noise ratio (SNR) and zero-point uncertainties. The g' , r' , and i' band magnitudes are tabulated in Table 2 and the corresponding light curves are shown in Figure 1.

The optical magnitudes need to be corrected for the galactic extinction using the relations $A_g = 1.161 \times A_V$, $A_r = 0.843 \times A_V$, and $A_i = 0.639 \times A_V$ (Schlegel et al. 1998), where A_V is derived from the hydrogen column density as $A_V = N_H / 2.21 \times 10^{21} \text{ cm}^{-2}$ (Güver & Özel 2009) and $N_H = 8.6 \times 10^{21} \text{ cm}^{-2}$ (Tominaga et al. 2020). Only observations with $\text{SNR} > 5$ were included in our subsequent analyses.

3. RESULTS

In this section, we investigate the time delays and flux correlation between the Comptonization flux and optical emission, and perform SED fitting for the X-ray and optical bands.

3.1. Time delays

Time delays between different radiation bands provide direct probes of the physical scales and underlying mechanisms in accreting systems. The delay between optical and X-ray emission can reflect the viscous timescale of the accretion disk, revealing how fluctuations propagate inward and outward (e.g., Weng et al. 2021; You et al. 2023). In the case of X-ray reprocessing, such delays correspond to the light travel time from the central X-ray source to the outer disk, offering constraints on the geometry and structure of this system.

As illustrated in Figure 1, a evident time delay can be found between the peaks of the optical and X-ray light curves. To quantitatively determine the time delay between the optical emission and Comptonization flux,

Table 1. Comptonization flux of MAXI J1348-630

MJD	$\log F_{\text{comp}}$ ($\text{erg s}^{-1} \text{cm}^{-2}$)	MJD	$\log F_{\text{comp}}$ ($\text{erg s}^{-1} \text{cm}^{-2}$)
58637.39	-7.98 ± 0.029	58663.38	-7.59 ± 0.008
58637.52	-7.93 ± 0.016	58663.38	-7.59 ± 0.008
58637.65	-7.94 ± 0.019	58663.58	-7.58 ± 0.010
58637.82	-7.97 ± 0.015	58663.58	-7.58 ± 0.010
58639.08	-7.89 ± 0.010	58665.07	-7.62 ± 0.009
58644.24	-7.57 ± 0.008	58665.21	-7.68 ± 0.004
58648.48	-7.52 ± 0.008	58665.21	-7.68 ± 0.004
58649.25	-7.50 ± 0.007	58665.36	-7.62 ± 0.010
58649.38	-7.52 ± 0.011	58665.36	-7.62 ± 0.010
58650.67	-7.48 ± 0.009	58667.06	-7.65 ± 0.010
58650.84	-7.49 ± 0.007	58667.06	-7.65 ± 0.010
58650.97	-7.60 ± 0.007	58667.22	-7.64 ± 0.009
58651.86	-7.48 ± 0.010	58667.35	-7.65 ± 0.011
58652.12	-7.57 ± 0.026	58670.06	-7.70 ± 0.011
58652.13	-7.50 ± 0.011	58670.06	-7.70 ± 0.011
58652.76	-7.46 ± 0.008	58670.20	-7.69 ± 0.010
58652.82	-7.50 ± 0.008	58670.20	-7.69 ± 0.010
58652.96	-7.52 ± 0.015	58672.28	-7.70 ± 0.011
58653.88	-7.51 ± 0.011	58672.28	-7.70 ± 0.011
58654.08	-7.50 ± 0.012	58672.45	-7.72 ± 0.008
58654.11	-7.49 ± 0.008	58672.45	-7.72 ± 0.008
58654.71	-7.49 ± 0.008	58672.61	-7.71 ± 0.011
58654.81	-7.50 ± 0.007	58672.61	-7.71 ± 0.011
58654.94	-7.49 ± 0.010	58672.74	-7.62 ± 0.005
58655.37	-7.50 ± 0.005	58672.74	-7.62 ± 0.005
58655.57	-7.48 ± 0.009	58673.94	-7.78 ± 0.010
58655.70	-7.50 ± 0.006	58673.94	-7.78 ± 0.010
58657.06	-7.52 ± 0.008	58675.33	-7.76 ± 0.008
58657.06	-7.52 ± 0.008	58675.33	-7.76 ± 0.008
58657.19	-7.52 ± 0.007	58676.92	-7.82 ± 0.011
58657.33	-7.52 ± 0.006	58677.25	-7.86 ± 0.011
58659.84	-7.56 ± 0.016	58679.82	-7.86 ± 0.010
58659.84	-7.56 ± 0.016	58681.81	-7.88 ± 0.013
58661.32	-7.57 ± 0.007	58681.95	-7.91 ± 0.022
58661.32	-7.57 ± 0.007	58684.66	-7.96 ± 0.012
58661.46	-7.55 ± 0.008	58687.17	-8.00 ± 0.020
58661.46	-7.55 ± 0.008	58689.79	-8.19 ± 0.019
58661.59	-7.57 ± 0.008	58691.41	-8.22 ± 0.022
58661.59	-7.57 ± 0.008	58691.54	-8.33 ± 0.012
58663.22	-7.60 ± 0.008	58691.68	-8.33 ± 0.034
58663.22	-7.60 ± 0.008	58693.40	-8.52 ± 0.020

Table 2. Observed optical magnitudes of MAXI J1348-630

MJD	g'	r'	i'
58624.64	18.96 ± 0.14	17.95 ± 0.08	17.12 ± 0.11
58630.44	17.83 ± 0.09	16.94 ± 0.04	16.30 ± 0.04
58631.08	17.76 ± 0.10	16.88 ± 0.07	16.25 ± 0.07
58634.77	17.42 ± 0.10	16.60 ± 0.07	15.94 ± 0.07
58639.42	17.13 ± 0.06	16.37 ± 0.03	15.67 ± 0.06
58640.01	17.21 ± 0.08	16.35 ± 0.05	15.72 ± 0.07
58640.48	16.99 ± 0.02	-	15.47 ± 0.01
58640.95	17.15 ± 0.11	16.29 ± 0.07	15.66 ± 0.10
58641.96	17.07 ± 0.08	16.20 ± 0.06	15.54 ± 0.05
58643.70	-	16.38 ± 0.10	15.78 ± 0.07
58643.95	17.21 ± 0.09	16.40 ± 0.05	15.75 ± 0.08
58645.36	17.25 ± 0.03	16.45 ± 0.08	15.78 ± 0.02
58647.71	17.28 ± 0.14	16.46 ± 0.09	15.81 ± 0.08
58648.37	17.27 ± 0.10	16.46 ± 0.09	15.82 ± 0.04
58649.82	17.26 ± 0.14	16.44 ± 0.14	15.75 ± 0.13
58651.40	17.26 ± 0.09	16.49 ± 0.10	15.85 ± 0.06
58652.82	17.36 ± 0.12	16.50 ± 0.10	15.82 ± 0.09
58655.36	17.37 ± 0.10	16.54 ± 0.06	15.87 ± 0.06
58656.97	17.37 ± 0.08	16.52 ± 0.09	15.87 ± 0.08
58662.00	17.46 ± 0.09	16.62 ± 0.07	15.96 ± 0.07
58664.96	17.48 ± 0.08	16.65 ± 0.08	16.00 ± 0.08
58673.72	17.62 ± 0.10	16.76 ± 0.07	16.09 ± 0.09
58675.74	17.58 ± 0.12	16.73 ± 0.12	16.05 ± 0.1
58680.75	17.59 ± 0.19	16.84 ± 0.06	16.23 ± 0.09
58686.83	17.99 ± 0.10	17.11 ± 0.06	16.49 ± 0.07
58693.80	18.44 ± 0.12	17.65 ± 0.06	16.99 ± 0.07
58697.80	18.73 ± 0.12	17.81 ± 0.10	17.05 ± 0.12
58698.80	18.82 ± 0.16	17.84 ± 0.10	17.06 ± 0.09

we employed an interpolated cross-correlation function (ICCF) analysis (for detailed methods of ICCF, see [You et al. 2023](#)). To estimate the uncertainties of the time delays, we performed the flux randomization/random subset sampling (FR/RSS) method, which takes into account the measurement uncertainties and those arising from the sampling cadence. The ICCF results are presented in Figure 2. We found that X-ray Comptonization light curve lags behind the g' band by a peak delay of $\tau_p = 8.56^{+2.02}_{-2.05}$ days and the centroid delay of $\tau_c = 8.73^{+1.32}_{-1.32}$ days (uncertainties are at the 1σ level). For the r' band, the delays are $\tau_p = 8.33^{+1.35}_{-1.15}$ days and $\tau_c = 8.35^{+1.19}_{-1.15}$ days, while for the i' band, they are $\tau_p = 8.54^{+1.32}_{-2.02}$ days and $\tau_c = 8.54^{+1.22}_{-1.17}$ days. These results clearly indicate that the light curves of the three monochromatic optical bands are simultaneous, and that the X-ray emission lags behind the optical emission by approximately 8.5 days during the mini-outburst.

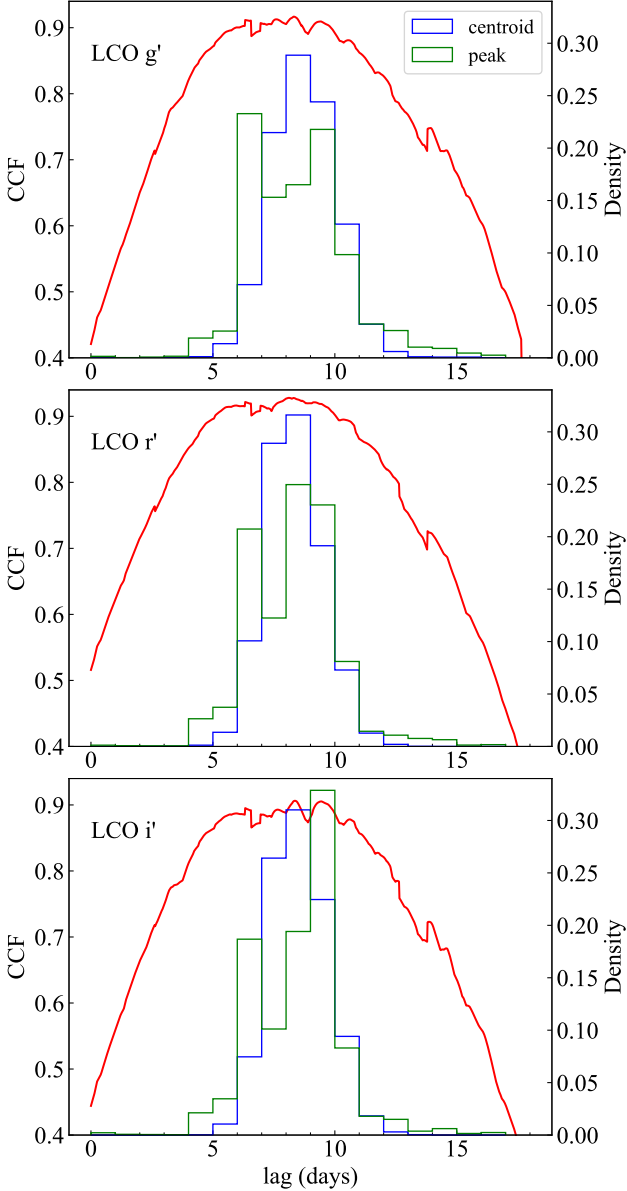


Figure 2. Cross-correlation analysis between the Comptonization flux and different optical bands (g' , r' , and i' bands for the top, middle, and bottom panels, respectively). In all panels, the red line indicates the cross-correlation function (left axis), and the green and blue histograms are the cross-correlation peak delay distribution and the centroid delay distribution (right axis).

3.2. Flux correlations

Russell et al. (2006) suggested that the power-law correlations between the X-ray and optical flux ($F_{\text{opt}} \propto F_X^\beta$) can be used to probe the origin of optical emission in LMXBs. A slope of $\beta \sim 0.7$ typically indicates synchrotron emission from a compact jet (Gallo et al. 2003); $\beta \sim 0.5$ implies that optical emission results from X-ray

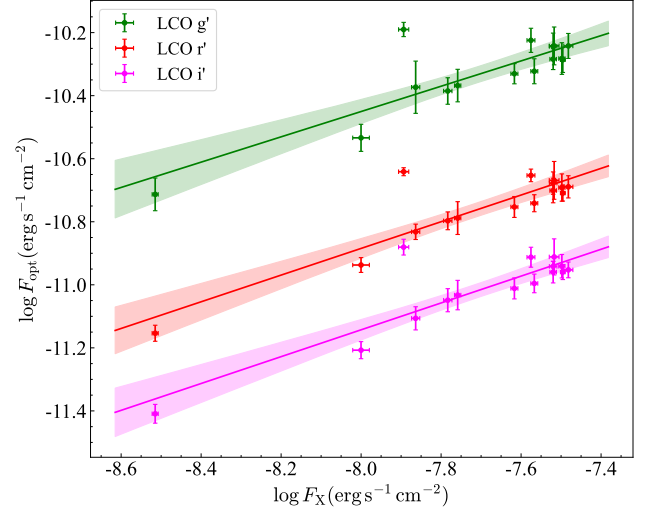


Figure 3. The power-law correlation between the Comptonization flux and different optical bands (see the legend). The solid lines are the best fits, and the shaded regions indicate uncertainties at the 1σ level.

reprocessing in the outer accretion disc (van Paradijs & McClintock 1994); and $\beta \sim 0.25$ suggests a viscously heated accretion disc origin of optical emission (e.g., Yang et al. 2022). Recent investigations of the correlations between X-ray Comptonization and optical flux in MAXI J1820+070 were conducted by You et al. (2023), which found that $\beta \sim 1.0$ during the rising hard state, indicating a steeper correlation compared to those observed in the hard state of LMXBs, but no correlation was detected during the decaying hard state. These findings pose a challenge to our understanding of the origin of the optical emission.

In this study, we selected quasi-simultaneous X-ray and optical observations (within one day) and fitted the data using the `linmix` package¹, a Bayesian-based linear regression tool that takes flux errors into account. As shown in the top panel of Figure 3, a clear power-law correlation is observed between the Comptonization flux and the optical flux in mini-outburst of MAXI J1348-630, with best-fit slopes of $\beta = 0.40 \pm 0.097$, 0.42 ± 0.082 , and 0.43 ± 0.083 for g' , r' , and i' bands, respectively.

3.3. SED fitting

We constructed SEDs using quasi-simultaneous optical and X-ray data (within one day) to investigate the multi-wavelength emission during the mini-outburst of MAXI J1348-630. In total, 13 quasi-simultaneous SEDs were collected. The SEDs were modeled using `tbabs*diskir` in `XSPEC`, where `tbabs` accounts for X-

¹ <https://linmix.readthedocs.io/en/latest/>

ray absorption (Wilms et al. 2000), and `diskir` represents an irradiated disk model, which considers the effects of inner disk and corona irradiation on the outer accretion disk (Gierliński et al. 2008, 2009). Note that `tbabs` does not account for optical extinction; therefore, the optical data were corrected for extinction following the method described in Section 2.2. The corrected optical data were then converted into XSPEC format using `ftflx2xsp` module². In the fittings, we fixed the neutral hydrogen column density toward MAXI J1348–630 at $N_{\text{H}} = 8.6 \times 10^{21} \text{ cm}^{-2}$ (Tominaga et al. 2020). There are nine parameters in the irradiated disk model; we fixed $f_{\text{in}} = 0.1$ and $r_{\text{irr}} = 1.1$ as the default value for the hard state (Gierliński et al. 2008, 2009). After testing, we found $L_{\text{c}}/L_{\text{d}}$ was poorly constrained, so we fixed it to the typical hard state value of 5 (e.g., Rodi et al. 2021; Özbey Arabacı et al. 2022; Echiburú-Trujillo et al. 2024). Finally, six parameters were free to fit the SEDs.

We found that all 13 quasi-simultaneous SEDs can be well fitted by the irradiated disk model, and the best-fit parameters are reported in Table 3. As a representative case, in Figure 4, we displayed the SED and corresponding fitting results at MJD 58643, when happens to have quasi-simultaneous radio observations at 5.5 and 9 GHz (Carotenuto et al. 2021, more about the radio emission is discussed in Section 4.1). The well-fitting results clearly illustrate that the irradiated disk model can successfully account for the optical and X-ray emission of MAXI J1348–630 during its mini-outburst. The consistency of good fits throughout the mini-outburst further strengthens the interpretation that the optical emission is dominated by the irradiated outer disk.

4. DISCUSSIONS

4.1. Origin of Optical Emission

Our results show that the optical emission significantly precedes the X-ray emission (see Figure 2) by ~ 8.5 days, which can be naturally interpreted by the DIM (Lasota 2001; Dubus et al. 2001; Goodwin et al. 2020; You et al. 2023; Du et al. 2025). When the inward-moving heating front reaches the inner edge of the accretion disk, the optical emission soon peaks. However, the accretion flow continues to propagate inward due to viscous dissipation, causing the mass accretion rate at the truncation radius to reach its maximum at a later time (You et al. 2023; Du et al. 2025). Given that the Comptonization luminosity scales approximately with the square of the accretion rate at truncation radius,

therefore, the time delay between X-ray and optical light curves is the natural consequence of the DIM. On the other hand, You et al. (2024) reported that there is no significant time delay between the X-ray and radio emission during the mini-outburst, implying that the optical emission should also lead radio emission by several days. The jet model predicts that the time delay between radio and optical emission is about tens of minutes (e.g., Tetarenko et al. 2019). Therefore, the analysis of the time delay supports the interpretation that the optical emission originates from the disk, rather than the jet.

Carotenuto et al. (2021) reported a flat radio spectrum of MAXI J1348–630 during the mini-outburst (i.e., $\alpha \sim 0$, where the radio flux density follows $S_{\nu} \propto \nu^{\alpha}$), which is the signature of self-absorbed synchrotron emission (Blandford & Königl 1979; Fender 2001), implying the presence of a compact radio jet. It has been suggested that the flat self-absorbed synchrotron spectrum of the compact jet could extend to near-infrared or even optical regimes (Fender 2001; Russell et al. 2013), beyond which the jet becomes optically thin, exhibiting a spectral index of $-1 < \alpha < -0.5$. To estimate the contribution of the jet to the optical emission, we plotted the quasi-simultaneous radio data of 5.5 and 9 GHz presented by Carotenuto et al. (2021) in Figure 4 (green dots). The frequency at which self-absorbed synchrotron radiation transitions from optically thick to optically thin remains highly uncertain (e.g., Russell et al. 2013). Therefore, for simplicity, we fit the radio data with a single power-law ($\alpha = -0.03$, corresponding to a spectral index of 0.97 in Figure 4) and extrapolate it to the optical band (green dotted line). Given that the synchrotron radiation of the jet is possibly optically thin in the optical band, the contribution of the jet to optical emission must be lower than the green dotted line. As shown in the figure, this line still lies significantly below the optical data, suggesting that the contribution of the jet to the optical emission during the mini-outburst of MAXI J1348–630 is negligible. In fact, the optical emission has been well explained by the irradiated disk model, indicating that it originates from the irradiation of the disk by the inner X-rays. The irradiation effect is also incorporated in the DIM (e.g., You et al. 2023; Du et al. 2025).

The slope of the correlation between optical and X-ray emission, $\beta \sim 0.4$, is significantly lower than the predicted value of 0.7 based on synchrotron emission from the jet (Gallo et al. 2003), but lies between the predicted value of ~ 0.25 based on viscously heated disk and ~ 0.5 predicted by X-ray reprocessing (see Russell et al. 2006, and the references therein). As discussed above, the optical emission from the jet is negligible, suggesting

² <https://heasarc.gsfc.nasa.gov/docs/software/lheasoft/help/ftflx2xsp.html>

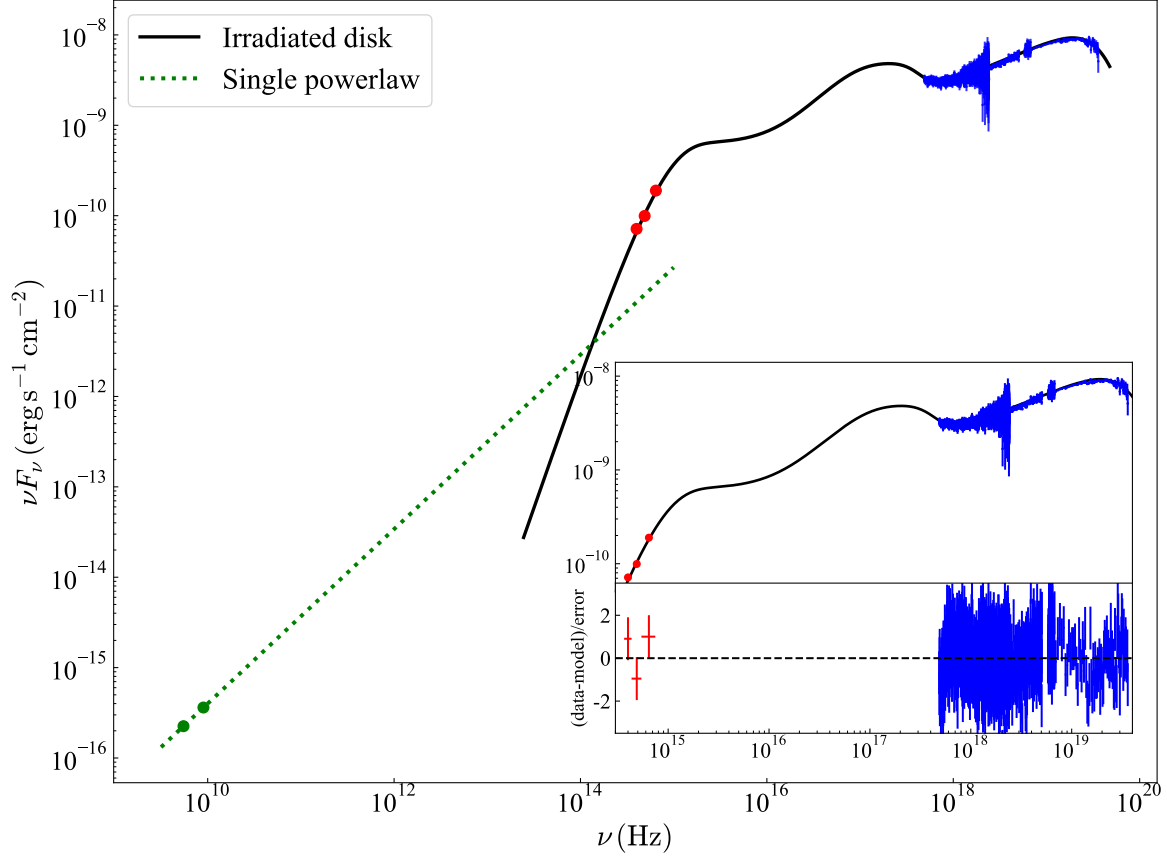


Figure 4. Best-fit unabsorbed SED of MAXI J1348-630 at MJD 58643. The blue and red data points correspond to the observation of Insight-HXMT and LCO. The radio data (green points) were observed by ACTA, presented by [Carotenuto et al. \(2021\)](#). The black line represents the best-fit of `tbabs*diskirr`. The green dotted line is a power-law fit to radio data. The bottom-right panel is a zoom-in of the X-ray and optical fits, along with the fit residuals.

Table 3. Best-fit values and errors at 90% confidence level of parameters in SED fitting

MJD	kT_{in} (keV)	Γ	kT_e (keV)	f_{out} (10^{-3})	$\log(r_{\text{out}}/r_{\text{in}})$	Norm (10^5)	$\chi^2/\text{d.o.f}$
58643	$0.179^{+0.002}_{-0.003}$	$1.632^{+0.008}_{-0.008}$	$49.94^{+2.95}_{-2.48}$	$8.2^{+9.9}_{-3.7}$	$3.81^{+0.14}_{-0.14}$	$2.74^{+0.21}_{-0.14}$	1417/1277
58648	$0.181^{+0.003}_{-0.002}$	$1.671^{+0.007}_{-0.007}$	$58.89^{+3.82}_{-3.43}$	$6.9^{+3.9}_{-2.5}$	$3.79^{+0.09}_{-0.11}$	$2.97^{+0.14}_{-0.19}$	1473/1277
58649	$0.188^{+0.004}_{-0.005}$	$1.663^{+0.013}_{-0.013}$	$54.35^{+5.99}_{-4.81}$	$6.7^{+11.5}_{-3.7}$	$3.84^{+0.22}_{-0.24}$	$2.56^{+0.27}_{-0.23}$	1308/1277
58651	$0.188^{+0.004}_{-0.004}$	$1.655^{+0.011}_{-0.011}$	$52.64^{+4.72}_{-3.77}$	$7.4^{+9.1}_{-3.4}$	$3.76^{+0.13}_{-0.14}$	$2.81^{+0.28}_{-0.23}$	1379/1277
58652	$0.186^{+0.003}_{-0.003}$	$1.664^{+0.009}_{-0.009}$	$56.60^{+4.78}_{-3.94}$	$5.1^{+6.8}_{-2.4}$	$3.84^{+0.17}_{-0.17}$	$2.82^{+0.22}_{-0.19}$	1433/1277
58655	$0.185^{+0.003}_{-0.003}$	$1.665^{+0.008}_{-0.008}$	$58.51^{+4.35}_{-3.55}$	$4.9^{+4.8}_{-1.9}$	$3.82^{+0.13}_{-0.13}$	$2.86^{+0.18}_{-0.16}$	1390/1277
58657	$0.183^{+0.004}_{-0.003}$	$1.658^{+0.009}_{-0.010}$	$60.60^{+5.53}_{-4.66}$	$6.5^{+7.5}_{-2.7}$	$3.78^{+0.13}_{-0.15}$	$2.92^{+0.24}_{-0.23}$	1367/1277
58661	$0.171^{+0.003}_{-0.003}$	$1.671^{+0.010}_{-0.010}$	$90.56^{+20.97}_{-13.36}$	$5.7^{+7.6}_{-2.4}$	$3.73^{+0.13}_{-0.16}$	$3.52^{+0.32}_{-0.28}$	1360/1277
58665	$0.164^{+0.003}_{-0.003}$	$1.652^{+0.010}_{-0.010}$	$74.26^{+11.25}_{-8.46}$	$7.8^{+10.3}_{-3.3}$	$3.68^{+0.13}_{-0.15}$	$3.67^{+0.34}_{-0.30}$	1280/1277
58673	$0.162^{+0.004}_{-0.004}$	$1.631^{+0.010}_{-0.010}$	$68.74^{+8.24}_{-6.40}$	$8.5^{+13.0}_{-4.0}$	$3.76^{+0.16}_{-0.17}$	$2.65^{+0.28}_{-0.23}$	1365/1277
58675	$0.163^{+0.003}_{-0.003}$	$1.615^{+0.009}_{-0.009}$	$61.96^{+6.06}_{-5.00}$	$8.3^{+15.0}_{-4.3}$	$3.78^{+0.19}_{-0.19}$	$2.63^{+0.20}_{-0.18}$	1214/1277
58679	$0.158^{+0.004}_{-0.004}$	$1.635^{+0.010}_{-0.010}$	$77.82^{+13.49}_{-9.50}$	$9.3^{+16.5}_{-5.5}$	$3.75^{+0.23}_{-0.23}$	$2.45^{+0.28}_{-0.23}$	1379/1277
58687	$0.154^{+0.007}_{-0.007}$	$1.641^{+0.021}_{-0.021}$	$112.96^{+162.68}_{-38.06}$	$9.5^{+13.0}_{-4.2}$	$3.75^{+0.15}_{-0.16}$	$2.02^{+0.53}_{-0.47}$	1341/1277

that $\beta \sim 0.4$ could be achieved when both irradiation and viscous heating contribute to the optical emission. In fact, the irradiated disk model adopted in the SED fitting accounts for both the effects of irradiation and viscous heating. The consistent results from the correlation analysis and SED fitting indicate that the optical emission during the mini-outburst of MAXI J1348–630 originates from the disk rather than from a jet. Note that this slope is remarkably similar to that observed in MAXI J1820+070 during its mini-outburst (Bright et al. 2025; Yang et al. 2025). However, based on the SED fittings of MAXI J1820+070, Özbey Arabacı et al. (2022) suggested that the jet contributes significantly to its optical emission. Although MAXI J1820+070 exhibits a similar correlation slope to MAXI J1348–630, SED fittings yield different results, indicating that relying solely on flux correlation analysis may be insufficient to conclusively determine the origin of optical emission in LMXBs.

In summary, our analysis favors the interpretation that the optical emission of MAXI J1348–630 during the mini-outburst originates from the disk rather than the jet, and DIM is the key to understanding the optical emission that precedes the X-rays and the observed SED.

4.2. Color-magnitude diagram

To investigate the color evolution of MAXI J1348–630 during its mini-outburst, we present the color-magnitude diagram (CMD, Maitra & Bailyn 2008) based on the magnitudes of the g' and i' bands. CMD of MAXI J1348–630 are shown in Figure 5. It can be seen that at lower luminosities, the evolution of MAXI J1348–630 roughly follows the expectation of a single-temperature blackbody disk with increasing temperature (for more details about the methodology of CMD, see Maitra & Bailyn 2008), but as the luminosity increases, it gradually begins to deviate. This trend is quite similar to that observed in some other LMXBs (e.g., Russell et al. 2011; Poutanen et al. 2014; Zhang et al. 2019), and we suggest that this deviation may be due to the fact that the single-temperature blackbody disk oversimplifies the temperature profile of the accretion disk. However, MAXI J1348–630 never exhibits a prominent “hook” feature (see figure in Russell et al. 2011; Poutanen et al. 2014), which has been interpreted as a signature of jet contribution. This further supports our argument that the optical emission of MAXI J1348–630 is dominated by the disk rather than by the jet. Özbey Arabacı et al. (2022), when fitting the SED of MAXI J1820+070 during its mini-outburst using an irradiated disk model, found that a good fit could only

be achieved by including an additional power-law component extending from the radio to the optical band, which was interpreted as a contribution of the jet. For comparison, we also plotted the color evolution of the first mini-outburst of MAXI J1820+070 (MJD from 58560 to 58670), where optical data are taken from Sai et al. (2021). The trend of MAXI J1820+070 is similar to that of MAXI J1348–630, but its color index is redder overall, which may be due to a lower disk temperature or the contribution of the jet.

We also analyzed the optical data of MAXI J1348–630 during its main outburst and present its color evolution in Figure 5 for comparison. Unlike some other LMXBs (e.g., Russell et al. 2011; Zhang et al. 2019; Saikia et al. 2023), the evolutionary trend of MAXI J1348–630 during the main outburst does not follow the expectation of a single-temperature blackbody disk; however, this trend appears to be consistent with the high-luminosity portion of the mini-outburst. On the other hand, Weng et al. (2021) suggested that the optical emission of MAXI J1348–630 during the main outburst originates from the accretion disk, and reported an optical and X-ray correlation slope of ~ 0.38 . This value is very similar to that found in the mini-outburst, which may imply that the optical origins during the main outburst and the mini-outburst are possibly the same. In fact, it has been suggested that the mini-outburst and the main outburst are driven by the same mechanism (e.g., Yan & Yu 2017; Cúneo et al. 2020), but more research is required to investigate the relationship between the mini-outburst and the main outburst.

4.3. On the state transition

As observed in most mini-outbursts of LMXBs (Patruno et al. 2016; Zhang et al. 2019; Özbey Arabacı et al. 2022; Saikia et al. 2023, e.g.), MAXI J1348–630 remained in the LHS throughout its mini-outburst without undergoing a state transition (Zhang et al. 2020a; Carotenuto et al. 2021). The truncated disk model serves as the paradigm for understanding state transitions (Done et al. 2007; Yuan & Narayan 2014), in which a geometrically thin, optically thick accretion disk is truncated at a certain radius. Inside the truncation radius, the accretion disk transitions to a hot, optically thin, geometrically thick accretion flow, often modeled as an advection-dominated accretion flow (ADAF) or a corona. As the source transitions from the LHS to the HSS, the truncation radius gradually moves inward toward the innermost stable circular orbit (ISCO), significantly increasing its thermal disk emission. Concurrently, the hot accretion flow (or corona) diminishes in size and luminosity. The reverse processes occur during

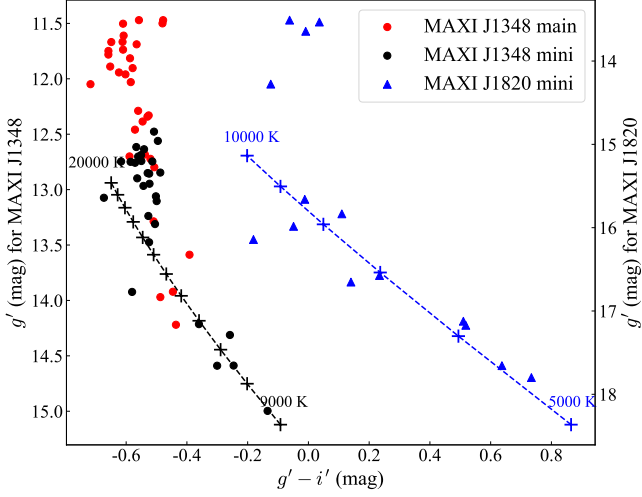


Figure 5. Color-magnitude diagram of MAXI J1348-630 and MAXI J1820+070. The magnitudes in this figure have been corrected for extinction. The left and right y-axes represent the g' magnitudes of MAXI J1348-630 and MAXI J1820+070, respectively. Red and black points denote the main outburst and mini-outburst of MAXI J1348-630, while blue triangles represent the mini-outburst of MAXI J1820+070. The two dashed lines are the theoretical curves of a blackbody disk for each source (see Maitra & Bailyn 2008, for more details), and the plus signs mark the temperature of the blackbody at intervals of 1000 K.

the transition back to the LHS, where the disk starts to recede, reducing the thermal disk emission, and the Comptonized power-law component once again dominates the X-ray spectrum. This process for the soft-to-hard state transition was recently confirmed with the observations of MAXI J1820+070 (You et al. 2023). Dai et al. (2023) found that the disk of MAXI J1348-630 actually moved inward during the mini-outburst, but never reached the ISCO, consequently failing to transition to the soft state (see also, García et al. 2019).

The mini-outburst of MAXI J1348-630 resembles a “failed outburst” (Zhang et al. 2020a). Recent studies

have revealed that failed outbursts, during the several tens of days after the onset of the outburst, exhibit X-ray light curves, HID tracks, and timing properties that are nearly indistinguishable from those of full outbursts, suggesting a common physical mechanism at the onset (Kosenkov et al. 2020; Alabarta et al. 2021). However, Lucchini et al. (2023) suggested that X-ray variability, especially changes in power spectral hue, tends to evolve 10 to 40 days prior to a state transition. In contrast, such an evolution is not observed in failed outbursts. This finding could serve as a predictive tool for anticipating state transitions and may provide new insights into the physical mechanisms of state transitions. On the other hand, in the optical and infrared bands, Alabarta et al. (2021) found that failed outbursts are brighter than full outbursts, and Yang et al. (2025) showed that optical and X-ray light curves dip before the hard-to-soft transition. Therefore, optical emission may be the key to understanding state transitions.

Although state transitions of mini-outbursts have been reported in several LMXBs (e.g., GR 1739-278 and MAXI J1535-571, Yan & Yu 2017; Cúneo et al. 2020), the lack of optical observations precludes a direct comparison with MAXI J1348-630 to further investigate state transitions. In fact, optical emission of many mini-outbursts has been missed due to their low luminosity and/or the lack of regular optical monitoring. We look forward to more sustained, high-cadence, multi-wavelength monitoring of LMXBs, which will enable further investigation of the state transition of LMXBs.

- 1 This work is supported by the National Program on Key
- 2 Research and Development Project 2021YFA0718500;
- 3 by Natural Science Foundation of China (NSFC) grants
- 4 12322307, 12361131579, and 12273026; by Xiaomi Founda-
- 5 tion / Xiaomi Young Talents Program.

REFERENCES

- Alabarta, K., Méndez, M., García, F., et al. 2022, *MNRAS*, 514, 2839, doi: [10.1093/mnras/stac1533](https://doi.org/10.1093/mnras/stac1533)
- Alabarta, K., Altamirano, D., Méndez, M., et al. 2021, *MNRAS*, 507, 5507, doi: [10.1093/mnras/stab2241](https://doi.org/10.1093/mnras/stab2241)
- Belloni, T. M., & Motta, S. E. 2016, in *Astrophysics and Space Science Library*, Vol. 440, *Astrophysics of Black Holes: From Fundamental Aspects to Latest Developments*, ed. C. Bambi, 61, doi: [10.1007/978-3-662-52859-4_2](https://doi.org/10.1007/978-3-662-52859-4_2)
- Blandford, R. D., & Königl, A. 1979, *ApJ*, 232, 34, doi: [10.1086/157262](https://doi.org/10.1086/157262)
- Brennan, S. J., & Fraser, M. 2022, *A&A*, 667, A62, doi: [10.1051/0004-6361/202243067](https://doi.org/10.1051/0004-6361/202243067)
- Bright, J. S., Fender, R., Russell, D. M., et al. 2025, *MNRAS*, 541, 1851, doi: [10.1093/mnras/staf1098](https://doi.org/10.1093/mnras/staf1098)
- Brown, T. M., Baliber, N., Bianco, F. B., et al. 2013, *PASP*, 125, 1031, doi: [10.1086/673168](https://doi.org/10.1086/673168)
- Carotenuto, F., Corbel, S., Tremou, E., et al. 2021, *MNRAS*, 504, 444, doi: [10.1093/mnras/stab864](https://doi.org/10.1093/mnras/stab864)

- Chen, Y. P., Ma, X., Huang, Y., et al. 2019, *The Astronomer's Telegram*, 12470, 1
- Cúneo, V. A., Alabarta, K., Zhang, L., et al. 2020, *MNRAS*, 496, 1001, doi: [10.1093/mnras/staa1606](https://doi.org/10.1093/mnras/staa1606)
- Dai, X., Kong, L., Bu, Q., et al. 2023, *MNRAS*, 521, 2692, doi: [10.1093/mnras/stad714](https://doi.org/10.1093/mnras/stad714)
- Done, C., Gierliński, M., & Kubota, A. 2007, *A&A Rv*, 15, 1, doi: [10.1007/s00159-007-0006-1](https://doi.org/10.1007/s00159-007-0006-1)
- Du, D., You, B., Yan, Z., et al. 2025, arXiv e-prints, arXiv:2507.00578, doi: [10.48550/arXiv.2507.00578](https://doi.org/10.48550/arXiv.2507.00578)
- Dubus, G., Hameury, J. M., & Lasota, J. P. 2001, *A&A*, 373, 251, doi: [10.1051/0004-6361:20010632](https://doi.org/10.1051/0004-6361:20010632)
- Echiburú-Trujillo, C., Tetarenko, A. J., Haggard, D., et al. 2024, *ApJ*, 962, 116, doi: [10.3847/1538-4357/ad1a10](https://doi.org/10.3847/1538-4357/ad1a10)
- Fender, R. 2006, in *Compact stellar X-ray sources*, ed. W. H. G. Lewin & M. van der Klis, Vol. 39, 381–419, doi: [10.48550/arXiv.astro-ph/0303339](https://doi.org/10.48550/arXiv.astro-ph/0303339)
- Fender, R. P. 2001, *MNRAS*, 322, 31, doi: [10.1046/j.1365-8711.2001.04080.x](https://doi.org/10.1046/j.1365-8711.2001.04080.x)
- Gallo, E., Fender, R. P., & Pooley, G. G. 2003, *MNRAS*, 344, 60, doi: [10.1046/j.1365-8711.2003.06791.x](https://doi.org/10.1046/j.1365-8711.2003.06791.x)
- García, J. A., Tomsick, J. A., Sridhar, N., et al. 2019, *ApJ*, 885, 48, doi: [10.3847/1538-4357/ab384f](https://doi.org/10.3847/1538-4357/ab384f)
- Gierliński, M., Done, C., & Page, K. 2008, *MNRAS*, 388, 753, doi: [10.1111/j.1365-2966.2008.13431.x](https://doi.org/10.1111/j.1365-2966.2008.13431.x)
- . 2009, *MNRAS*, 392, 1106, doi: [10.1111/j.1365-2966.2008.14166.x](https://doi.org/10.1111/j.1365-2966.2008.14166.x)
- Goodwin, A. J., Russell, D. M., Galloway, D. K., et al. 2020, *MNRAS*, 498, 3429, doi: [10.1093/mnras/staa2588](https://doi.org/10.1093/mnras/staa2588)
- Güver, T., & Özel, F. 2009, *MNRAS*, 400, 2050, doi: [10.1111/j.1365-2966.2009.15598.x](https://doi.org/10.1111/j.1365-2966.2009.15598.x)
- Hameury, J. M. 2020, *Advances in Space Research*, 66, 1004, doi: [10.1016/j.asr.2019.10.022](https://doi.org/10.1016/j.asr.2019.10.022)
- Hjellming, R. M., & Johnston, K. J. 1988, *ApJ*, 328, 600, doi: [10.1086/166318](https://doi.org/10.1086/166318)
- Homan, J., & Belloni, T. 2005, *Ap&SS*, 300, 107, doi: [10.1007/s10509-005-1197-4](https://doi.org/10.1007/s10509-005-1197-4)
- Homan, J., Buxton, M., Markoff, S., et al. 2005, *ApJ*, 624, 295, doi: [10.1086/428722](https://doi.org/10.1086/428722)
- Homan, J., Wijnands, R., van der Klis, M., et al. 2001, *ApJS*, 132, 377, doi: [10.1086/318954](https://doi.org/10.1086/318954)
- Jana, A., Debnath, D., Chatterjee, D., et al. 2020, *ApJ*, 897, 3, doi: [10.3847/1538-4357/ab9696](https://doi.org/10.3847/1538-4357/ab9696)
- Kosenkov, I. A., Veledina, A., Suleimanov, V. F., & Poutanen, J. 2020, *A&A*, 638, A127, doi: [10.1051/0004-6361/201936143](https://doi.org/10.1051/0004-6361/201936143)
- Lasota, J.-P. 2001, *NewAR*, 45, 449, doi: [10.1016/S1387-6473\(01\)00112-9](https://doi.org/10.1016/S1387-6473(01)00112-9)
- Lucchini, M., Ten Have, M., Wang, J., et al. 2023, *ApJ*, 958, 153, doi: [10.3847/1538-4357/ad0294](https://doi.org/10.3847/1538-4357/ad0294)
- Maitra, D., & Bailyn, C. D. 2008, *ApJ*, 688, 537, doi: [10.1086/592029](https://doi.org/10.1086/592029)
- Markoff, S., Falcke, H., & Fender, R. 2001, *A&A*, 372, L25, doi: [10.1051/0004-6361:20010420](https://doi.org/10.1051/0004-6361:20010420)
- Mitsuda, K., Inoue, H., Koyama, K., et al. 1984, *PASJ*, 36, 741
- Negoro, H., Mihara, T., Nakajima, M., et al. 2019, *The Astronomer's Telegram*, 12838, 1
- Özbey Arabacı, M., Kalemci, E., Dinçer, T., et al. 2022, *MNRAS*, 514, 3894, doi: [10.1093/mnras/stac1574](https://doi.org/10.1093/mnras/stac1574)
- Patruno, A., Maitra, D., Curran, P. A., et al. 2016, *ApJ*, 817, 100, doi: [10.3847/0004-637X/817/2/100](https://doi.org/10.3847/0004-637X/817/2/100)
- Poutanen, J., Veledina, A., & Revnivtsev, M. G. 2014, *MNRAS*, 445, 3987, doi: [10.1093/mnras/stu1989](https://doi.org/10.1093/mnras/stu1989)
- Remillard, R. A., & McClintock, J. E. 2006, *ARA&A*, 44, 49, doi: [10.1146/annurev.astro.44.051905.092532](https://doi.org/10.1146/annurev.astro.44.051905.092532)
- Rodi, J., Tramacere, A., Onori, F., et al. 2021, *ApJ*, 910, 21, doi: [10.3847/1538-4357/abdfd0](https://doi.org/10.3847/1538-4357/abdfd0)
- Russell, D. M., Baglio, C. M., & Lewis, F. 2019a, *The Astronomer's Telegram*, 12439, 1
- Russell, D. M., Fender, R. P., Hynes, R. I., et al. 2006, *MNRAS*, 371, 1334, doi: [10.1111/j.1365-2966.2006.10756.x](https://doi.org/10.1111/j.1365-2966.2006.10756.x)
- Russell, D. M., Maitra, D., Dunn, R. J. H., & Fender, R. P. 2011, *MNRAS*, 416, 2311, doi: [10.1111/j.1365-2966.2011.19204.x](https://doi.org/10.1111/j.1365-2966.2011.19204.x)
- Russell, D. M., Markoff, S., Casella, P., et al. 2013, *MNRAS*, 429, 815, doi: [10.1093/mnras/sts377](https://doi.org/10.1093/mnras/sts377)
- Russell, T., Anderson, G., Miller-Jones, J., et al. 2019b, *The Astronomer's Telegram*, 12456, 1
- Rykoff, E. S., Miller, J. M., Steeghs, D., & Torres, M. A. P. 2007, *ApJ*, 666, 1129, doi: [10.1086/520329](https://doi.org/10.1086/520329)
- Sai, H., Wang, X., Wu, J., et al. 2021, *MNRAS*, 504, 4226, doi: [10.1093/mnras/stab1162](https://doi.org/10.1093/mnras/stab1162)
- Saikia, P., Russell, D. M., Pirbhoy, S. F., et al. 2023, *ApJ*, 949, 104, doi: [10.3847/1538-4357/acc8cc](https://doi.org/10.3847/1538-4357/acc8cc)
- Sanna, A., Uttley, P., Altamirano, D., et al. 2019, *The Astronomer's Telegram*, 12447, 1
- Schlegel, D. J., Finkbeiner, D. P., & Davis, M. 1998, *ApJ*, 500, 525, doi: [10.1086/305772](https://doi.org/10.1086/305772)
- Shakura, N. I., & Sunyaev, R. A. 1973, *A&A*, 24, 337
- Sunyaev, R. A., & Titarchuk, L. G. 1980, *A&A*, 86, 121
- Tetarenko, A. J., Sivakoff, G. R., Miller-Jones, J. C. A., et al. 2019, *MNRAS*, 482, 2950, doi: [10.1093/mnras/sty2853](https://doi.org/10.1093/mnras/sty2853)
- Tominaga, M., Nakahira, S., Shidatsu, M., et al. 2020, *ApJL*, 899, L20, doi: [10.3847/2041-8213/abaaaa](https://doi.org/10.3847/2041-8213/abaaaa)
- van Paradijs, J., & McClintock, J. E. 1994, *A&A*, 290, 133
- Weng, S.-S., Cai, Z.-Y., Zhang, S.-N., et al. 2021, *ApJL*, 915, L15, doi: [10.3847/2041-8213/ac0a7b](https://doi.org/10.3847/2041-8213/ac0a7b)

- Wilms, J., Allen, A., & McCray, R. 2000, *ApJ*, 542, 914, doi: [10.1086/317016](https://doi.org/10.1086/317016)
- Yan, Z., & Yu, W. 2017, *MNRAS*, 470, 4298, doi: [10.1093/mnras/stx1562](https://doi.org/10.1093/mnras/stx1562)
- Yang, P., Zhang, G., Russell, D. M., et al. 2022, *MNRAS*, 514, 234, doi: [10.1093/mnras/stac1120](https://doi.org/10.1093/mnras/stac1120)
- . 2025, arXiv e-prints, arXiv:2507.00532, doi: [10.48550/arXiv.2507.00532](https://doi.org/10.48550/arXiv.2507.00532)
- Yatabe, F., Negoro, H., Nakajima, M., et al. 2019, *The Astronomer’s Telegram*, 12425, 1
- You, B., Yang, S.-k., Yan, Z., Cao, X., & Zdziarski, A. A. 2024, *ApJL*, 969, L33, doi: [10.3847/2041-8213/ad5b50](https://doi.org/10.3847/2041-8213/ad5b50)
- You, B., Tuo, Y., Li, C., et al. 2021, *Nature Communications*, 12, 1025, doi: [10.1038/s41467-021-21169-5](https://doi.org/10.1038/s41467-021-21169-5)
- You, B., Cao, X., Yan, Z., et al. 2023, *Science*, 381, 961, doi: [10.1126/science.abo4504](https://doi.org/10.1126/science.abo4504)
- Yuan, F., & Narayan, R. 2014, *ARA&A*, 52, 529, doi: [10.1146/annurev-astro-082812-141003](https://doi.org/10.1146/annurev-astro-082812-141003)
- Zdziarski, A. A., & Gierliński, M. 2004, *Progress of Theoretical Physics Supplement*, 155, 99, doi: [10.1143/PTPS.155.99](https://doi.org/10.1143/PTPS.155.99)
- Zhang, G. B., Bernardini, F., Russell, D. M., et al. 2019, *ApJ*, 876, 5, doi: [10.3847/1538-4357/ab12dd](https://doi.org/10.3847/1538-4357/ab12dd)
- Zhang, L., Altamirano, D., Cúneo, V. A., et al. 2020a, *MNRAS*, 499, 851, doi: [10.1093/mnras/staa2842](https://doi.org/10.1093/mnras/staa2842)
- Zhang, S.-N., Li, T., Lu, F., et al. 2020b, *Science China Physics, Mechanics, and Astronomy*, 63, 249502, doi: [10.1007/s11433-019-1432-6](https://doi.org/10.1007/s11433-019-1432-6)